Article

Cell Reports

Crosstalk between Regulatory T Cells and Tumor-Associated Dendritic Cells Negates Anti-tumor Immunity in Pancreatic Cancer

Graphical Abstract

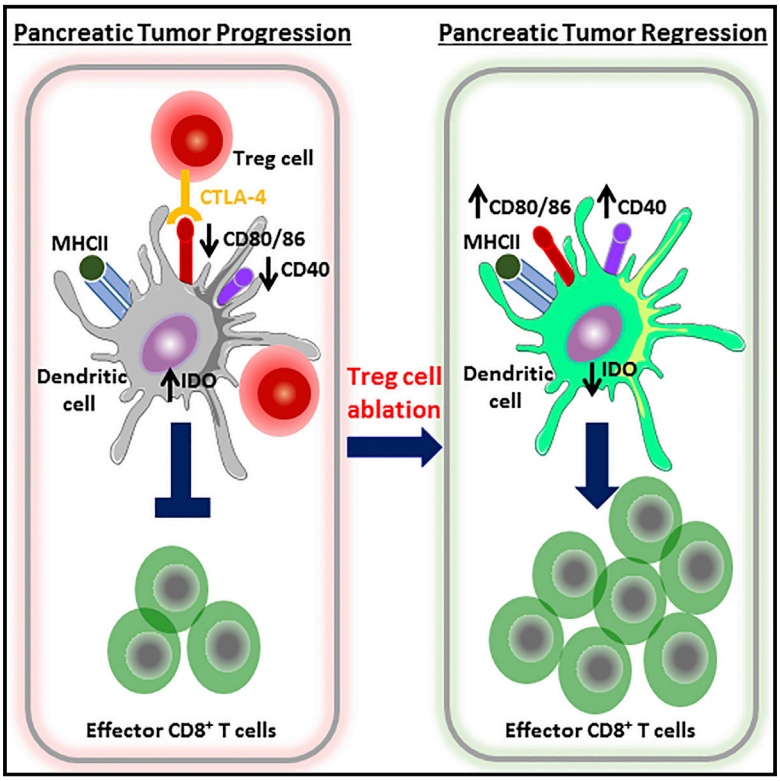

Highlights

- Treg cells restrain tumor-associated DC expansion and immunogenicity
- Treg cell depletion elicits effective anti-tumor immunity in pancreatic cancer
- Anti-tumor effects of Treg cell depletion are dependent on $CD8^+$ T cell activation

Authors

Jung-Eun Jang, Cristina H. Hajdu, Caroline Liot, George Miller, Michael L. Dustin, Dafna Bar-Sagi

Correspondence

michael.dustin@kennedy.ox.ac.uk (M.L.D.), dafna.bar-sagi@nyumc.org (D.B.-S.)

In Brief

Pancreatic tumors recruit dendritic cells that can switch between preventing or promoting immune responses. Jang et al. show that regulatory T cells are responsible for instructing the dendritic cells to prevent anti-tumor immunity. Removing the regulatory T cell subset allows dendritic cells to induce a potent anti-tumor immune response.

Jang et al., 2017, Cell Reports *20*, 558–571
July 18, 2017
http://dx.doi.org/10.1016/j.celrep.2017.06.062

CellPress

OPEN ACCESS
CellPress

Cell Reports
Article

Crosstalk between Regulatory T Cells and Tumor-Associated Dendritic Cells Negates Anti-tumor Immunity in Pancreatic Cancer

Jung-Eun Jang,[1,2] Cristina H. Hajdu,[3] Caroline Liot,[2] George Miller,[4,5] Michael L. Dustin,[1,6,*] and Dafna Bar-Sagi[2,7,*]
[1]Skirball Institute of Biomolecular Medicine
[2]Department of Biochemistry and Molecular Pharmacology
[3]Department of Pathology
[4]Department of Surgery
[5]Department of Cell Biology
New York University School of Medicine, New York, NY 10016, USA
[6]Kennedy Institute, Nuffield Department of Orthopedics, Rheumatology and Musculoskeletal Sciences, University of Oxford, Headington, Oxford OX3 7BN, UK
[7]Lead Contact
*Correspondence: michael.dustin@kennedy.ox.ac.uk (M.L.D.), dafna.bar-sagi@nyumc.org (D.B.-S.)
http://dx.doi.org/10.1016/j.celrep.2017.06.062

SUMMARY

Regulatory T (Treg) cell infiltration constitutes a prominent feature of pancreatic ductal adenocarcinoma (PDA). However, the immunomodulatory function of Treg cells in PDA is poorly understood. Here, we demonstrate that Treg cell ablation is sufficient to evoke effective anti-tumor immune response in early and advanced pancreatic tumorigenesis in mice. This response is dependent on interferon-γ (IFN-γ)-producing cytotoxic $CD8^+$ T cells. We show that Treg cells engage in extended interactions with tumor-associated $CD11c^+$ dendritic cells (DCs) and restrain their immunogenic function by suppressing the expression of costimulatory ligands necessary for $CD8^+$ T cell activation. Consequently, tumor-associated $CD8^+$ T cells fail to display effector activities when Treg cell ablation is combined with DC depletion. We propose that tumor-infiltrating Treg cells can promote immune tolerance by suppressing tumor-associated DC immunogenicity. The therapeutic manipulation of this axis might provide an effective approach for the targeting of PDA.

INTRODUCTION

Pancreatic ductal adenocarcinoma (PDA) is one of the most lethal human malignancies (Ryan et al., 2014). A hallmark of PDA is a pronounced fibroinflammatory stroma, which contributes to disease initiation and progression (Stromnes et al., 2014; Vonderheide and Bayne, 2013). The inflammatory infiltrates that populate PDA lesions are predominantly immunosuppressive in nature and include tumor-associated macrophages, myeloid-derived suppressor cells (MDSCs), γδ T cells, and regulatory T (Treg) cells (Daley et al., 2016; Hiraoka et al., 2006; Markowitz et al., 2015). Murine models of oncogenic Ras-driven PDA recapitulate many of these immune signatures (Bayne et al., 2012; Clark et al., 2007; Daley et al., 2016). Understanding the mechanisms underlying the immunosuppressive effects of these cell types is therefore essential to develop effective immunotherapies for the treatment of PDA.

$CD4^+$ $Foxp3^+$ Treg cells are crucial for the maintenance of immunological self-tolerance and have the ability to actively impede the anti-tumor immune response in a variety of cancer types (Josefowicz et al., 2012). In PDA, the accumulation of Treg cells in the tumor microenvironment occurs during the pre-invasive stage of the disease (Clark et al., 2007; Hiraoka et al., 2006). A high frequency of Treg cells in the pre-neoplastic pancreas is associated with poor prognosis and reduced survival in murine and human PDA (Hiraoka et al., 2006; Tang et al., 2014). Accordingly, Treg cell depletion in combination with conventional PDA treatment strategies has been shown to enhance cancer-specific T cell activation in preclinical studies (Keenan et al., 2014; Leao et al., 2008).

A variety of mechanisms for Treg cell-mediated suppression of effector T cell responses have been proposed, including direct elimination of effector T cells and competition with effector T cells for access to antigen-presenting dendritic cells (DCs) (Josefowicz et al., 2012; Kim et al., 2007; Nishikawa and Sakaguchi, 2010). Treg cells have also been shown to suppress DC immunogenicity in in vitro co-culture systems (Cederbom et al., 2000; Onishi et al., 2008). However, the precise mechanism of Treg cell-dependent immune modulation in PDA remains poorly understood.

Here, we demonstrate that Treg cells promote PDA development through the suppression of $CD8^+$ T cell-dependent anti-tumor immunity. Intratumoral Treg cells engage in prolonged interactions with tumor-associated $CD11c^+$ DCs and reduce their expression of molecules important for T cell activation. Treg cell ablation leads to the restoration of immunogenic tumor-associated $CD11c^+$ DCs and increases in $CD8^+$ T cell activation. Importantly, Treg cell ablation results in an inhibition in tumor growth that is dependent on interferon-γ (IFN-γ) expressed by $CD8^+$ T cells. Thus, the targeting of Treg cells in

PDA may facilitate anti-tumor immunity by harnessing the immune-stimulatory potential of tumor-associated DCs.

RESULTS

Treg Cells Are Required for Pancreatic Tumorigenesis

To discern the functional role of Treg cells in the development of pancreatic neoplasia, we employed an orthotopic implantation model in which primary *Kras*^{G12D}-expressing pancreatic ductal epithelial cells (*Kras*^{G12D}-PDECs) labeled with GFP (GFP-*Kras*^{G12D}-PDECs) are injected into the pancreata of syngeneic C57BL/6 wild-type (WT) mice (Pylayeva-Gupta et al., 2013). This model histologically recapitulates the pre-invasive stages of pancreatic intraepithelial neoplasia (PanIN) development and induces an intra-pancreatic immune response similar to that observed in the genetically engineered *p48-Cre*;*Kras*^{G12D} (KC) mouse model of pancreatic neoplasia (Clark et al., 2007; Pylayeva-Gupta et al., 2012). Furthermore, it preserves the natural histopathological features of disease development in that the lesions are produced in a focal manner and evolve in the context of normal pancreatic tissue. The implanted cells form a discernable mass (hereafter referred to as the tumor) that can be isolated along with the immediately adjacent parenchyma (hereafter referred to as the tumor microenvironment [TME]) and analyzed by flow cytometry and immunohistochemistry. We first assessed the frequency of tumor-associated Treg cells using the lineage specification transcription factor of Treg cells, forkhead box P3 (Foxp3) (Hori et al., 2003). Treg cells were readily detected within 1 week post-implantation of GFP-*Kras*^{G12D}-PDEC tumors and increased another ~2.5-fold by 5 weeks (Figures 1A and 1B), whereas Treg cells were rare in sham-injected or WT pancreata (data not shown). Importantly, Foxp3$^+$ Treg cells in the TME displayed elevated levels of the activation markers CD44 (Figure 1C), a hyaluronic acid receptor expressed on activated and memory Treg cell populations (Darrasse-Jèze et al., 2009); cytotoxic T-lymphocyte-associated protein 4 (CTLA-4), a Treg cell effector molecule (Wing et al., 2008); and programmed death 1 (PD-1), a negative costimulatory molecule (Keir et al., 2008), compared to tumor-draining pancreatic lymph nodes (Pan LNs) (Figures 1D and S1A). These data indicate that the development of pancreatic neoplasia is accompanied by the progressive accumulation of activated Treg cells.

Next, we examined the effect of Treg cell depletion on pancreatic neoplasia by implanting GFP-*Kras*^{G12D}-PDECs into the pancreata of *Foxp3*^{DTR} mice in which the human diphtheria toxin (DT) receptor (DTR) is expressed under the control of the *Foxp3* locus (Kim et al., 2007) (Figure 1E). DT treatment 1 week following orthotopic implantation resulted in >90% ablation of Treg cells within the pancreatic TME (Figure 1F) and a significant reduction in tumor growth (Figures 1G and 1H). DT treatment had no effect on the growth of GFP-*Kras*^{G12D}-PDECs implanted into WT mice (Figure S1B). The anti-tumor effect of Treg cell ablation persisted for 5 weeks post-implantation (Figure S1C). In addition, using an anti-CD25 neutralizing antibody to deplete Treg cells in KC mice, we observed a significant delay in disease progression (Figures S2A–S2C). Furthermore, Treg cell depletion in mice implanted with KPC cells derived from pancreata of a *Kras*$^{G12D/+}$;*Trp53*$^{R172H/+}$;*Pdx1-Cre* (KPC) mouse (Byrne and Vonderheide, 2016; Lo et al., 2015) was accompanied by a marked reduction in tumor volume and prolonged overall survival (Figures 1I and 1J). Together, these data demonstrate that Treg cells contribute to pancreatic tumor growth at both the early and late stages of disease progression.

Anti-tumor Immunity of Treg Cell Ablation Is Dependent on IFN-γ-Producing CD8$^+$ T Cells

Since anti-tumor responses require functional effector CD4$^+$ and CD8$^+$ T cells, we assessed the effect of Treg cell ablation on effector T cells in the TME, tumor-draining pancreatic lymph nodes (Pan LNs) and peripheral inguinal lymph nodes (iLNs). DT-induced Treg cell ablation resulted in the expansion and activation of tumor infiltrating CD4$^+$ and CD8$^+$ T cells at all sites (Figures 2A–2D and S3A–S3D). However, we have observed that intratumoral Treg cells express higher levels of effector molecules CTLA-4 and PD-1 (the latter being regulated by antigen exposure) relative to Treg cells in the tumor-draining Pan LNs and iLNs (Figures 1D and S1A). Thus, while we cannot formally exclude a contribution of effector CD8$^+$ T cells that have originated from tumor-draining Pan LNs to the anti-tumoral effect of DT-induced Treg cell depletion, the properties of the TME-associated Treg cells suggest a primary role for tumor-resident Treg cells in mediating immunosuppression.

We then sought to determine whether the anti-tumor effect of Treg cell ablation is mediated through CD4$^+$ or cytotoxic CD8$^+$ T cell activation. To this end, Treg cells were ablated alone or in combination with either CD4$^+$ or CD8$^+$ T cell depletion using CD4- or CD8-depleting antibody, and tumor growth was measured after 15 days. The depletion of CD4$^+$ T cells resulted in reduction of tumor growth similar to that observed in Treg cell ablation. However, the simultaneous depletion of CD4$^+$ T cells in combination with Treg cell ablation did not further decrease tumor growth compared to Treg cell depletion alone (Figure S3E), indicating that CD4$^+$ Foxp3$^-$ T cells are dispensable for the anti-tumor effect of Treg cell ablation. In contrast, the anti-tumor response observed in the setting of Treg cell ablation was reversed when combined with CD8$^+$ T cell depletion (Figure 2E). Since only CD8$^+$ T cells displayed a significant increase in the production of IFN-γ, a potent tumoricidal cytokine (Shankaran et al., 2001), we further investigated the role of IFN-γ in mediating the immune response to pancreatic neoplasia in orthotopic implant-bearing WT or *Foxp3*^{DTR} mice treated with a neutralizing anti-IFN-γ monoclonal antibody (mAb). While IFN-γ blockade in WT mice did not affect tumor growth, the concurrent administration of anti-IFN-γ antibody and DT to *Foxp3*^{DTR} mice abolished the inhibitory effect of Treg cell ablation on tumor growth (Figure 2F). Histological analysis revealed that the combined depletion of Treg cells and IFN-γ blockade was associated with the expansion of neoplastic lesions and a reduction in the frequency of apoptotic cells (Figures 2G–2I). Collectively, these results indicate that Treg cells may promote pancreatic neoplasia through the suppression of IFN-γ-producing activated CD8$^+$ T cells.

Treg Cells Engage CD11c$^+$ DCs within the TME

It is being increasingly recognized that interactions between Treg cells and DCs play a critical role in shaping the nature of

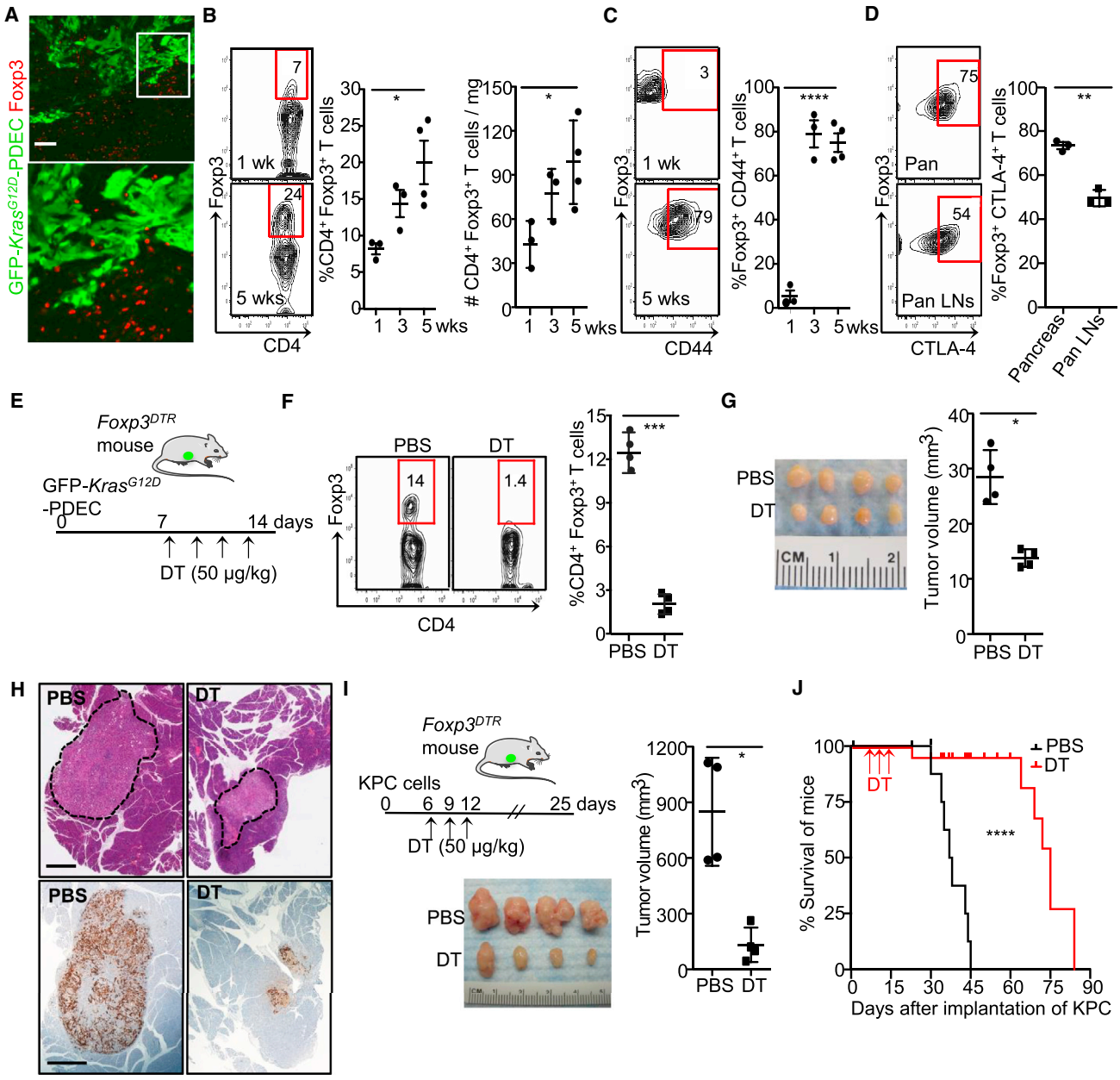

Figure 1. Intratumoral Treg Cells Promote Pancreatic Neoplastic Growth

GFP-*Kras*^{G12D}-PDECs were implanted (day 0) into the pancreata of syngeneic mice. Pancreata were analyzed at the time points indicated.

(A) Representative images of immunofluorescence staining for Foxp3 at 3 weeks post-implantation. Boxed region is magnified below (scale bar, 200 μm).

(B) Flow cytometric plots (left) and quantification (right) of the percentage and number of CD4$^+$ Foxp3$^+$ Treg cells (n = 3–4 mice).

(C) Flow cytometric plots (left) and quantification (right) of the expression of CD44 on Foxp3$^+$ Treg cells (n = 3–4 mice).

(D) Flow cytometric plots (left) and quantification (right) of the expression of CTLA-4 in Foxp3$^+$ Treg cells in pancreata and tumor-draining Pan LNs 5 weeks post-implantation (n = 3 mice).

(E–H) Schematic of the experimental design. The arrows indicate either PBS (control) or DT (50 μg/kg) was injected i.p. on days 7, 9, 11, and 13 after implantation of GFP-*Kras*^{G12D}-PDECs into pancreata of *Foxp3*^{DTR} mice. Analyses in (F) – (H) were performed 14 days after orthotopic implantation. (F) Flow cytometric plots (left) and quantification (right) of CD4$^+$ Foxp3$^+$ Treg cells (n = 4 mice). (G) Orthotopic pancreatic tumors (left) and quantification of tumor volume (right) (n = 4 mice). (H) Representative images of H&E staining (top) and GFP immunohistochemical staining (bottom) on sections from orthotopic pancreatic grafts. Scale bar, 1 mm.

(I and J) Schematic of the experimental design. Mice were analyzed on day 25 (I) or when moribund (J) after implantation of KPC cells. (I) Orthotopic pancreatic tumors (left) and quantification of tumor volume (right) from mice treated as shown (n = 4 mice). (J) Kaplan-Meier survival curves (****p < 0.0001, log-rank test) of mice implanted with KPC cells (n = 7–8 mice).

Data are representative of two or three independent experiments and are presented as mean ± SEM. *p < 0.05, **p < 0.01, ***p < 0.001, ****p < 0.0001. See also Figures S1 and S2.

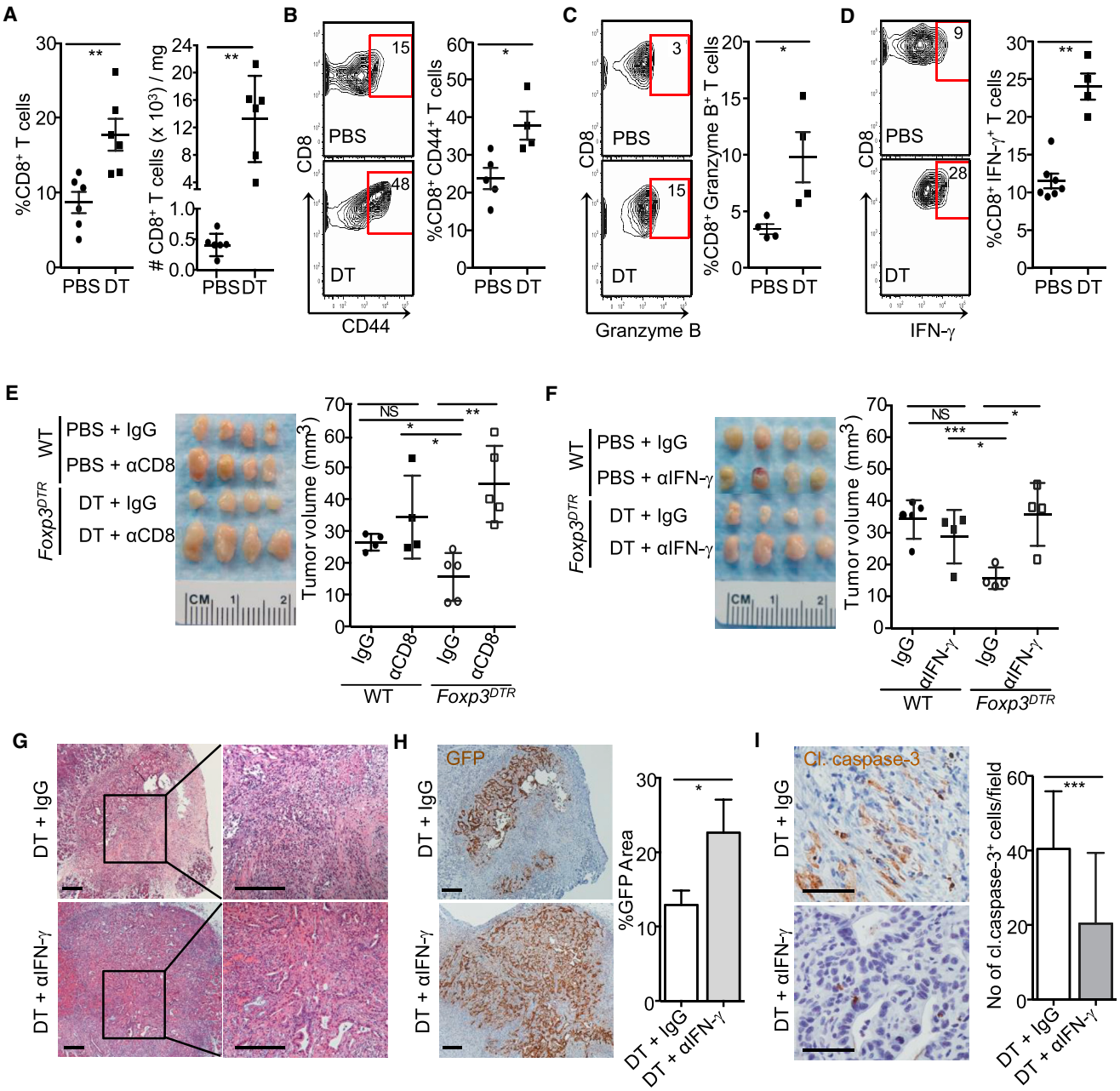

Figure 2. Anti-tumor Effect of Treg Cell Ablation Is Dependent on IFN-γ-Producing CD8$^+$ T Cells

For (A)–(D), either PBS or DT was injected as described in Figure 1E after implantation of GFP-*Kras*^{G12D}-PDECs into pancreata of *Foxp3*^{DTR} mice. Analyses were performed 14 days after orthotopic implantation.

(A) Quantification of the percentage and number of CD8$^+$ T cells (n = 4–7 mice).

(B–D) Flow cytometric plots (left) and quantification (right) of CD44- (B), granzyme B- (C), and IFN-γ- (D) expressing CD8$^+$ T cells in orthotopic pancreatic grafts (n = 4–7 mice).

(E) Either PBS or DT was injected i.p. 7 and 9 days post-implantation, and 250 μg rat IgG2a isotype or anti-CD8 (αCD8) antibody was injected 8 and 11 days after implantation of GFP-*Kras*^{G12D}-PDECs into pancreata of WT or *Foxp3*^{DTR} mice. Analysis was performed 15 days after orthotopic implantation. Orthotopic pancreatic tumors (left) and quantification of tumor volume (right) from mice treated as shown (n = 4–5 mice).

(F–I) Either PBS or DT was injected i.p. 7 and 9 days post-implantation, and 1 mg rat IgG1 isotype or anti-IFN-γ (αIFNγ) antibody was injected i.p. 9 days after implantation of GFP-*Kras*^{G12D}-PDECs into pancreata of WT or *Foxp3*^{DTR} mice. Analyses were performed 17 days after implantation. (F) Orthotopic pancreatic tumors (left) and quantification of tumor volume (right) from mice treated as shown (n = 4–5 mice). (G) Representative images of H&E staining on sections from orthotopic pancreatic grafts from *Foxp3*^{DTR} mice (left) with boxed regions shown at higher magnification (right). Scale bar, 100 μm. (H) Representative images of

(legend continued on next page)

the immune response (Onishi et al., 2008; Schildknecht et al., 2010; Tang et al., 2006). To test whether such interactions might be relevant to the immunosuppressive function of Treg cells in the context of pancreatic neoplasia, we employed intravital two-photon laser-scanning microscopy (TPLSM). We first assessed the prevalence within the TME of cells expressing CD11c, an integrin that is enriched in DCs, by implanting GFP-*Kras*^{G12D}-PDECs into the pancreata of *CD11c-EYFP* mice. CD11c$^+$ cells were rare in the normal pancreas but abundantly present within the neoplastic lesions formed by the orthotopically implanted GFP-*Kras*^{G12D}-PDECs (Figures 3A and 3B). Next, to analyze the spatiotemporal relationships between Treg and CD11c cells, GFP-*Kras*^{G12D}-PDECs were implanted into pancreata of *Foxp3-EGFP;CD11c-EYFP* mice. The majority of Foxp3$^+$ Treg cells were observed to directly contact resident CD11c$^+$ cells for at least 600 s, which was the duration of the time-lapse imaging (Figures 3C and 3D; Movie S1). Consistent with this co-localization pattern, immune staining of tumor sections showed that the majority of Foxp3$^+$ cells at the tumor margin are located in close proximity to cells expressing CD11c in mice implanted with GFP-*Kras*^{G12D}-PDECs or KPC cells (Figure 3H) and in KC mice (Figure 3I). By comparison, the interactions of CD8$^+$ T cells and CD11c$^+$ cells in orthotopic implant-bearing *CD8a-Cre;Rosa*^{tdtomato}*;CD11c-EYFP* mice had a shorter median duration of 100 s (Figures 3E–3G; Movie S2), which was extended to a median duration of 300 s in the setting of Treg cell ablation (Figures S4A–S4D; Movies S3 and S4). These observations raise the intriguing possibility that the interactions of Treg cells and CD8$^+$ T cells with antigen-bearing DCs are mutually limiting. We found no evidence for tumor-associated tertiary lymphoid structures (TA-TLSs) that contain Foxp3$^+$ Treg cells in either autochthonous or orthotopic pancreatic neoplasia (Figures S5A and S5B).

We next sought to characterize the nature of the CD11c-yellow fluorescent protein (YFP) cells recruited to tumors formed by the implanted GFP-*Kras*^{G12D}-PDECs. In agreement with a previous study reporting that, in *CD11c-EYFP* mice, the cells visualized by in vivo TPLSM are DCs (Lindquist et al., 2004), the CD11c-YFP cells expressed the DC markers CD11c, major histocompatibility complex (MHC) class II, and CD135 (Flt3) (Figure 4A). Expression of the macrophage marker F4/80 was detected only in a small subset (~8%) of the CD11c-YFP cells (Figure 4B). Notably, the CD11c-YFP cells located in the tumor-proximal region (within 50 μm of the tumor margin) exhibited lower motility and shorter displacement trajectory compared to CD11c-YFP cells located distally to the tumor (more than 50 μm from the tumor border) (Figures 4C–4E). Furthermore, the CD11c-YFP cells that were closely juxtaposed to the tumor had a dendritic morphology (Figure 3A).

In order to present antigen to Treg cells or effector T cells, DCs need to capture tumor antigens. To track the capacity of CD11c-YFP cells to take up tumor-derived material, bone marrow cells isolated from *CD11c-EYFP* mice were transplanted into lethally irradiated *p48-Cre;Kras*^{G12D}*;Rosa*^{tdTomato} (KCT) or control *p48-Cre;Rosa*^{tdTomato} (CT) mice, in which tdTomato is specifically expressed in the cells of the exocrine pancreas. We then looked for YFP$^+$ cells with intracellular tdTomato as a measure of pancreatic antigen uptake. Confocal microscopy in sections from KCT chimeras revealed tdTomato puncta in CD11c$^+$ cells within the neoplastic lesions (Figure 4F). Flow cytometry analysis also demonstrated the presence of tdTomato$^+$ CD45$^+$ cells in the pancreas and Pan LNs of both CT and KCT mice, respectively (Figure 4G). The tdTomato$^+$ CD45$^+$ cells expressed high levels of CD11c and MHC class II, indicating that the majority of cells in the tdTomato$^+$ CD45$^+$ population are likely to be DCs, as they bring tumor antigens to Pan LNs (Figure 4H).

Tumor-Associated CD11c$^+$ DCs Display a Tolerogenic Phenotype

The function of DCs depends on their maturation and activation status, which is defined by the expression of costimulatory molecules on their cell surface (Steinman et al., 2003). Expression levels of the maturation marker MHC class II (I-A^d) and the costimulatory molecules CD40 and CD86 (B7.2) on tumor-associated CD11c$^+$ DCs decreased over time in the pancreatic TME (Figure 5A). Similarly, in KC mice, expression of the maturation markers on CD11c$^+$ DCs was significantly lower in the pancreas than in the Pan LNs (Figure S6A) and in WT mice (Figure S6B). These observations indicate that tumor-associated DCs are immature or semi-mature DCs and as such are likely to drive a tolerogenic response during tumor progression. Consistent with this postulate, we found that tumor-associated DCs express indoleamine 2,3-dioxygenase (IDO), an enzyme implicated in the suppression of T cell responses and the promotion of immune tolerance (Munn and Mellor, 2016) (Figure 5B). Expression of IDO in DCs was also observed in human PDA, underscoring the potential pathophysiological relevance of this observation (Figure 5C).

The Tolerogenic Phenotype of Tumor-Associated CD11c$^+$ DCs Is Dependent on Treg Cells

Treg cells are endowed with the capacity to regulate costimulatory molecules on DCs through cell-contact-dependent mechanisms in vitro (Cederbom et al., 2000; Onishi et al., 2008; Qureshi et al., 2011). Given our observations that Treg cells engage in stable interactions with tumor-associated DCs, we investigated whether Treg cells may downregulate costimulatory molecules expressed on DCs. Implantation of GFP-*Kras*^{G12D}-PDECs into the pancreata of *Foxp3*^{DTR} mice followed by DT treatment was accompanied by a significant increase in the frequency of tumor-associated CD11c$^+$ DCs (Figures 6A and 6B). Furthermore, the expression levels of costimulatory molecules on tumor-associated CD11c$^+$ MHC class II$^+$ DCs were significantly increased in the absence of Foxp3$^+$ Treg cells (Figures 6C and S6C). In

GFP immunohistochemical staining (left) and quantification of the percentage of GFP-positive area (right) from orthotopic pancreatic grafts from *Foxp3*^{DTR} mice. Scale bar, 100 μm. (I) Representative images of cleaved (cl.) caspase-3 immunohistochemical staining (left) and quantification of the number of cleaved-caspase-3-positive cells per field (right) in orthotopic pancreatic grafts from *Foxp3*^{DTR} mice. Scale bar, 50 μm.
Data are representative of two independent experiments and are presented as mean ± SEM. *$p < 0.05$, **$p < 0.01$, ***$p < 0.001$. See also Figure S3.

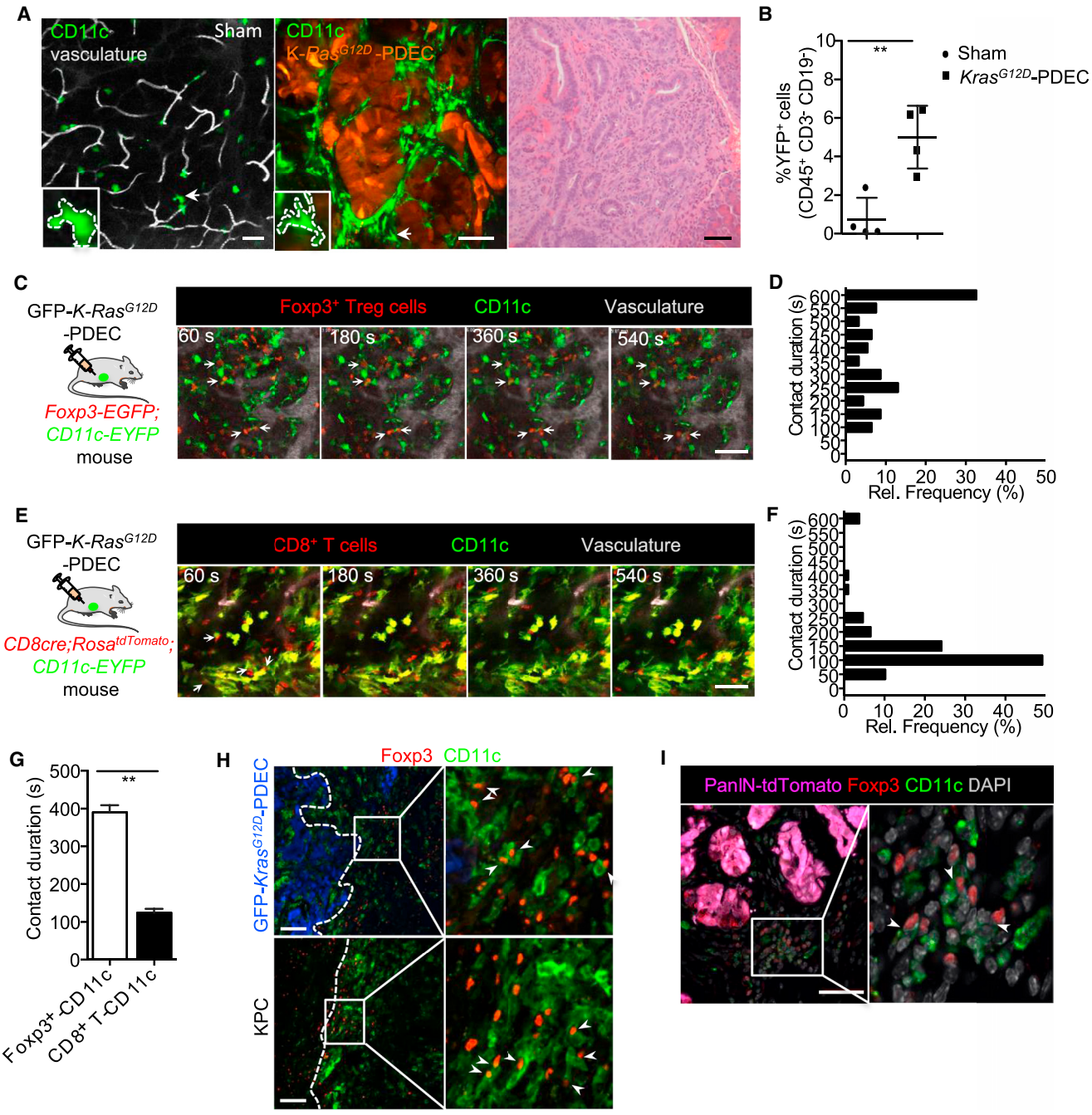

Figure 3. Dynamics of the Interaction between Treg Cells and Tumor-Associated CD11c$^+$ Cells in the Pancreatic TME

(A) Representative still images of CD11c$^+$ cells from intravital imaging from pancreata of *CD11c-EYFP* mice 4 weeks after injection of sham (Matrigel/PBS, 1:1, control) (left) and implantation of GFP-*Kras*^{G12D} -PDECs (middle). Vasculature (gray) was visualized by intravenously injection of Evan blue. Representative image of H&E staining on sections from orthotopic pancreatic grafts of GFP-*Kras*^{G12D}-PDEC implants (right). Scale bar, 50 μm.

(B) Flow cytometric analysis of YFP$^+$ population in orthotopic pancreatic grafts 10 days after implantation.

(C) The schematic illustrates the experimental system. Representative in vivo time-lapse images of contacts between Foxp3$^+$ and CD11c$^+$ cells in the pancreas of a *Foxp3-GFP;CD11c-YFP* mouse 3 weeks after implantation of GFP-*Kras*^{G12D}-PDECs. Scale bar, 50 μm.

(D) Analysis of contact duration between Foxp3$^+$ Treg cells and CD11c$^+$ cells (n = 3 mice).

(E) The schematic illustrates the experimental system. Representative in vivo time-lapse images of contacts between CD8$^+$ T and CD11c$^+$ cells in the pancreas of a *CD8a-Cre;Rosa*^{tdtomato}*;CD11c-EYFP* mouse 3 weeks after implantation of GFP-*Kras*^{G12D}-PDEC. Scale bar, 50 μm.

(F) Analysis of contact duration between CD8$^+$ T cells and CD11c$^+$ cells (n = 3 mice).

(G) Average contact duration of CD11c$^+$ cells with Foxp3$^+$ Treg cells or CD8$^+$ T cells, respectively (n = 3 mice).

(legend continued on next page)

addition, the expression of IDO in tumor-associated CD11c$^+$ DCs decreased following the ablation of Treg cells (Figure 6D and 6E). Collectively, these data suggest that Treg cells restrain the expansion of tumor-associated CD11c$^+$ DCs and their capacity to provide costimulation to T cells.

Treg Cells Act on Tumor-Associated CD11c$^+$ DCs to Impair Cytotoxic CD8$^+$ T Cell Activation

To determine whether there is a mechanistic link between the upregulation of DC activation markers and CD8$^+$ T cell activation in the context of Treg cell ablation, we performed Treg cell and DC co-depletion. WT or *Foxp3*^{DTR} mice were injected with DT on days 7 and 9 after implantation of GFP-*Kras*^{G12D}-PDEC in combination with administration of either control hamster immunoglobulin G (IgG) or anti-CD11c (N418) mAbs on days 7 and 10 (Figure 7A). This regimen resulted in ~95% and ~80% depletion of graft-associated Treg cells and DCs, respectively (Figures 7B and 7C). The effectiveness of DC depletion was confirmed by fluorescence-activated cell sorting (FACS) using a different clone of anti-CD11c antibody (HL3) to rule out the possible contribution of epitope masking to the analysis (Figure S7A). Whereas the depletion of CD11c$^+$ DCs alone did not affect tumor growth, the anti-tumor response observed in the setting of Treg cell ablation was reversed when combined with CD11c$^+$ DC depletion (Figure 7A). Furthermore, CD4$^+$ T cell activation was not impacted by combined Treg cell and DC ablation as compared with Treg cell ablation alone (Figures 7D and S7B). By contrast, ablation of Treg cells and DCs together fully reverted the proportion of CD8$^+$ T cells expressing CD44, granzyme B, and IFN-γ to levels observed in control grafts or CD11c$^+$ DC depletion alone (Figures 7E and S7C). Taken together, our results suggest that the cytotoxic CD8$^+$ T cell activation and effector activity observed in the setting of Treg cell ablation might be mediated by the functional maturation of tumor-associated CD11c$^+$ DCs.

DISCUSSION

Tumor-associated inflammation is a dynamic process involving the infiltration of multiple subtypes of leukocytes into the tumor stroma. A prominent component of the immune infiltrate is Treg cells, the presence of which correlates with poor clinical outcome in a variety of cancer types (Shang et al., 2015; Tang et al., 2014). In oncogenic *Kras*^{G12D}-induced pancreatic neoplasia, immune cell infiltration is an early and consistent event (Clark et al., 2007; Guerra et al., 2007). However, the exact role of Treg cells in pancreatic tumorigenesis is poorly understood. Here, we demonstrate that in the context of pancreatic neoplasia, intratumoral Treg cells play a tumor-promoting role by conferring immunosuppressive properties to tumor-associated CD11c$^+$ DCs. This limits the activation of tumor-infiltrating CD8$^+$ T cells, resulting in the reduction of IFN-γ production and a defect in tumor rejection.

The mechanisms by which Treg cells are recruited into the TME are not well understood. We have found that Treg cells accumulate around GFP-*Kras*^{G12D}-PDEC grafts within 1 week post-implantation. The short duration of this interval suggests that the neoplastic cells themselves may play a direct role in promoting Treg cell infiltration. Indeed, *Kras*^{G12D}-PDECs (unpublished data) and pancreatic cancer cells can produce high levels of the Treg cell attractants CXCL10, CCL5, and vascular endothelial growth factor (VEGF) that trigger the migration of Treg cells through interaction with the Treg cell-surface receptors CXCR3 (Lunardi et al., 2015), CCR5 (Tan et al., 2009), and neuropilin-1 (Hansen et al., 2012), respectively. Other cells within the TME, such as pancreatic stellate cells and tumor-infiltrating MDSCs, have also been reported to express high levels of Treg cell chemotactic factors, including CXCL10, CCL3, CCL4, and CCL5 (Lunardi et al., 2015; Schlecker et al., 2012). Thus, the intratumoral accumulation of all of the above cell types over the course of pancreatic tumor development may augment Treg cell infiltration and contribute to their expansion.

Our data demonstrate that the Treg cells that are recruited to the tumor graft are initially neuropilin-1^{hi} (data not shown) and CD44^{low} and are therefore most likely naive Treg cells of thymic origin that are selected on self-antigens (Weiss et al., 2012). At later stages, the vast majority of the intratumoral Treg cells exhibit a CD44^{high} memory/effector phenotype. It is not clear whether this shift reflects an in situ activation event or the recruitment of memory/effector Treg cells. The possibility that the activated phenotype is acquired in situ is supported by our observation that Treg cells engage in prolonged interactions with DCs within the TME. The DC-Treg cell interaction has been shown to potentiate Treg cell activation through either antigen recognition or the interaction of semaphorin 4A expressed on DCs with the Treg cell-expressed receptor neuropilin-1 (Delgoffe et al., 2013; Sarris et al., 2008). Of note, we have determined that neuropilin-1 is abundantly expressed in intratumoral Treg cells at all stages of pancreatic tumor progression (data not shown). Thus, the recruitment of CD44^{low} naive Treg cells that have low expression of CXCR3 and CCR5 could potentially be mediated through the chemotactic interaction between neuropilin-1 and tumor-derived VEGF.

Experimental depletion of Treg cells by administration of anti-CD25 antibodies or by DT administration to *Foxp3*^{DTR} mice has been shown to inhibit the growth of a variety of tumors, consistent with a role for Treg cells in suppressing anti-tumor immune responses (Bos et al., 2013; Joshi et al., 2015; Teng et al., 2010). However, the effector mechanisms by which Treg cells modulate anti-tumor immunity appear to vary between different tumor types. For example, in breast cancer, the anti-tumoral effect of Treg cell ablation is dependent on CD4$^+$ T cells and IFN-γ, pointing to a potential role for CD4$^+$ T cells as a non-redundant source of protective IFN-γ (Bos et al., 2013). In fibrosarcomas, the

(H and I) Representative images of immunofluorescence staining of Foxp3$^+$ and CD11c$^+$ cells from pancreata of WT mice 2 weeks after implantation of GFP-*Kras*^{G12D}-PDECs or KPC cells (H) and from a *p48-Cre*; *Kras*^{G12D}; *Rosa*^{tdTomato} (KCT) mouse (I). Boxed regions are magnified (right) with arrows indicating close proximity between cells expressing Foxp3 and CD11c. Scale bar, 200 μm.
Data are presented as mean ± SEM. **$p < 0.01$. See also Figures S4 and S5 and Movies S1, S2, S3, and S4.

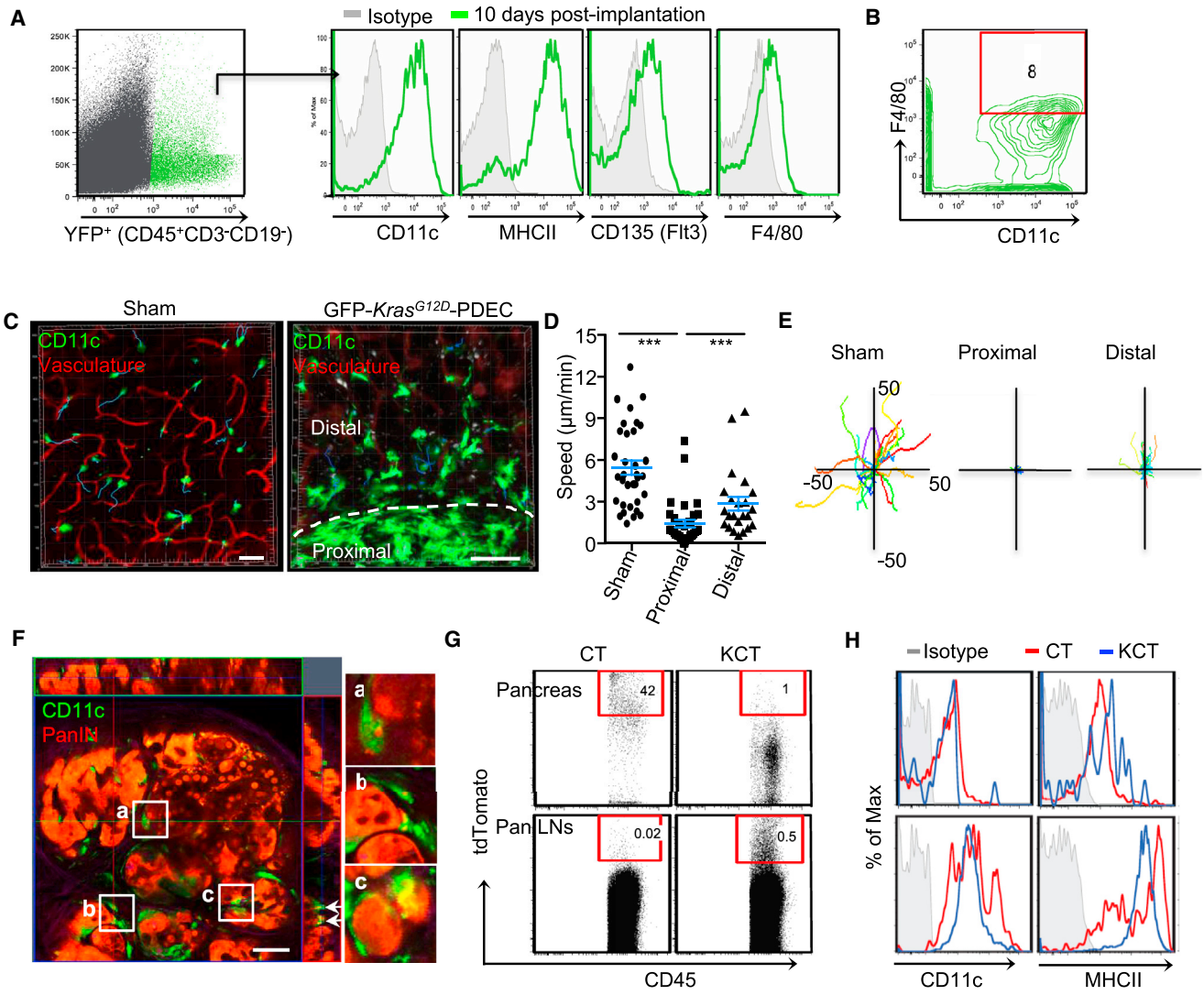

Figure 4. Tumor-Associated CD11c$^+$ DCs Display Reduced Local Migration and Bring Tumor Antigen to the Tumor-Draining LN

(A) Flow cytometric analysis of YFP$^+$ population 10 days after orthotopic pancreatic implantation of GFP-*Kras*^{G12D}-PDECs into *CD11c-EYFP* mice. After gating on the CD45$^+$ CD3$^-$ CD19$^-$ cell population, YFP$^+$ cells were analyzed using the cell-surface markers CD11c, MHC class II, CD135, and F4/80 and compared to respective isotype controls (gray).

(B) Flow cytometric analysis of CD11c$^+$F4/80$^+$ cells in the YFP$^+$ population.

(C) Representative still images of CD11c-YFP cells from sham injected (left) or GFP-*Kras*^{G12D}-PDECs implanted (right) 3 weeks post-implantation. The blue lines of each CD11c-YFP cell correspond to the displacement of CD11c$^+$ cells during a 10-min time lapse. Scale bar, 50 μm.

(D) Quantitative mean velocity of CD11c$^+$ cells in control, or proximal (within 50 μm) or distal (>50 μm) to the tumor border. Each dot represents an individual CD11c$^+$ cell (n = 3 mice).

(E) Displacement tracks of individual CD11c$^+$ cells in sham or proximal or distal to the tumor border. Each track represents the displacement of a cell from its starting point during a 10-min time lapse. Data are representative of at least three movies in three independent experiments.

(F) Representative still images from intravital imaging from pancreata of KCT chimeric mice generated by transplantation of bone marrow cells isolated from *CD11c-EYFP* mice. y-z and x-z cross sections are shown to the immediate right and above, respectively. White arrows indicate phagocytic tdTomato particles inside CD11c$^+$ cells. The boxed regions labeled a–c show CD11c$^+$ cells in which phagocytosis or co-expressed tdTomato particles are magnified (far right). Scale bar, 50 μm.

(G and H) Flow cytometric analysis of CD45$^+$tdTomato$^+$ cells (G) and expression of CD11c and MHC class II after gating on the CD45$^+$tdTomato$^+$ population compared to respective isotype controls (gray) (H) in the pancreas and Pan LNs of CT (control) or KCT mice.

Data are representative of three independent experiments and are presented as mean ± SEM. ***p < 0.001.

immune rejection of tumors following Treg cell depletion is CD8$^+$ T cell and IFN-γ dependent (Teng et al., 2010). Our findings indicate that similar effector mechanisms mediate the tumoricidal effects of Treg cell depletion on pancreatic tumors. The dependence on CD8$^+$ T cells is consistent with the observation that the net effect of CD4$^+$ T cells, which include Treg cells and

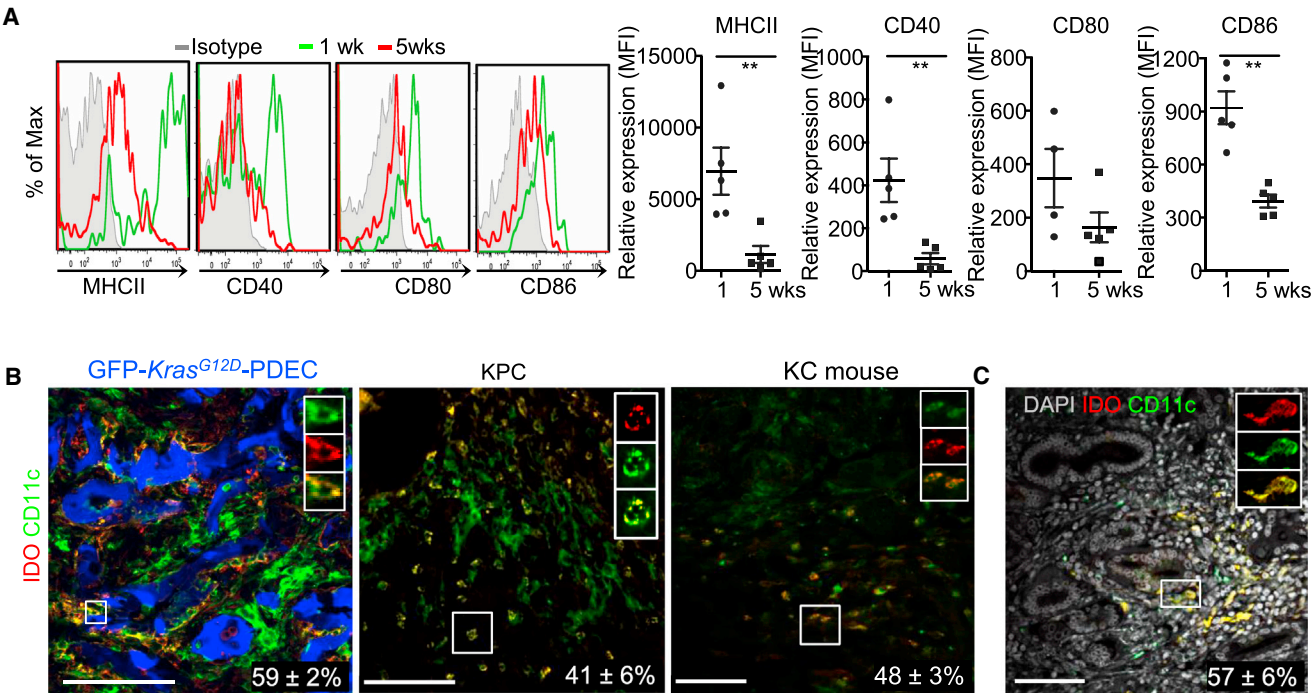

Figure 5. Tumor-Associated CD11c$^+$ DCs Display Reduced Maturation Markers and IDO Expression

(A) Relative surface expression levels of MHC class II, CD40, CD80, and CD86 on CD11c$^+$ cells from orthotopic pancreatic grafts at 1 and 5 weeks after implantation of GFP-*Kras*^{G12D}-PDECs compared to respective isotype controls (gray (n = 5 mice).

(B) Representative images of immunofluorescence staining of indoleamine 2,3-dioxygenase (IDO) and CD11c expression in pancreata from 2 weeks post-implantation of *GFP-Kras*^{G12D}- PDECs and KPC cells into WT and 4–6 month-old KC mice. Quantification of the percentage of IDO$^+$ cells in CD11c$^+$ cells per field is indicated in the bottom right-hand corner of the images. The boxed region is shown at higher magnification (insets). Scale bar, 100 μm.

(C) Representative images of immunofluorescence staining of IDO and CD11c expression in human PDA. Quantification of the percentage of IDO$^+$ cells in CD11c$^+$ cells per field is indicated in the bottom right-hand corner of the image. The boxed region is shown at higher magnification (inset) Scale bar, 100 μm.

Data are presented as mean ± SEM. **p < 0.01. See also Figure S6.

various conventional helper T cells, is to promote the onset of pancreatic neoplasia by modulating the activity of cytotoxic CD8$^+$ T cells. Ultimately, in human tumors, the potential therapeutic benefits of Treg cell targeting might be influenced by tumor-type specific mechanisms of immune tolerance.

Our findings identify DCs as critical targets of Treg cells to suppress anti-tumor immunity. DCs are essential determinants of the tumor immune response through the induction of immunogenicity or tolerance (Steinman et al., 2003). Tolerogenic DCs play a crucial role in immune tolerance through the inhibition of T cell proliferation or the induction of T cell anergy or Treg cell generation, resulting in diminished T cell-dependent anti-tumor immunity (Maldonado and von Andrian, 2010; Steinman et al., 2003). Tumor-associated DCs have been shown to display tolerogenic properties such as low expression of costimulatory molecules, low ability to process and present antigen to tumor-specific T cells, and low production of proinflammatory cytokines in a variety of cancer types (Bauer et al., 2014; Kim et al., 2007; Pinzon-Charry et al., 2005). The accumulation of tolerogenic tumor-associated DCs has been attributed to tumor- and TME-derived immunosuppressive factors such as VEGF, interleukin-10 (IL-10), transforming growth factor β (TGF-β), and PGE2 that modulate DC maturation and favor tolerogenic DC differentiation (Ghiringhelli et al., 2005; Scarlett et al., 2012; Yang and Lattime, 2003).

In addition, it has been proposed that Treg cell-mediated DC suppression could be mediated by direct cell-to-cell contact, leading to the downregulation of costimulatory molecules and apoptosis in DCs (Bauer et al., 2014; Boissonnas et al., 2010; Larmonier et al., 2007). Consistent with this idea, we have found that DCs interact with Treg cells in the pancreatic TME. The interaction between DCs and Treg cells has also been reported in breast cancer (Bauer et al., 2014), TA-TLSs in lung cancer (Joshi et al., 2015), and tumor-draining LNs (Boissonnas et al., 2010), suggesting that a contact-based crosstalk between these cell populations may be a general feature of tumor immune evasion.

The tolerogenic nature of DCs that are recruited to the pancreatic TME is also indicated by their expression of IDO. IDO-expressing DCs found at the tumor site and in tumor-draining LNs have been implicated in suppressing anti-tumor T cell responses to tumor-derived antigens and in promoting immune tolerance (Munn et al., 2002; Sharma et al., 2007). Mechanistically, the tolerogenic effect of IDO expression has been attributed to its enzymatic activity that leads to a reduction of tryptophan levels and the accumulation of metabolites of tryptophan catabolism, resulting in the inhibition of T cell proliferation and effector T cell toxicity (Munn and Mellor, 2016). A principal mechanism by which the expression of IDO in DCs can be upregulated is through the interaction of costimulatory molecules CD80 and CD86 with

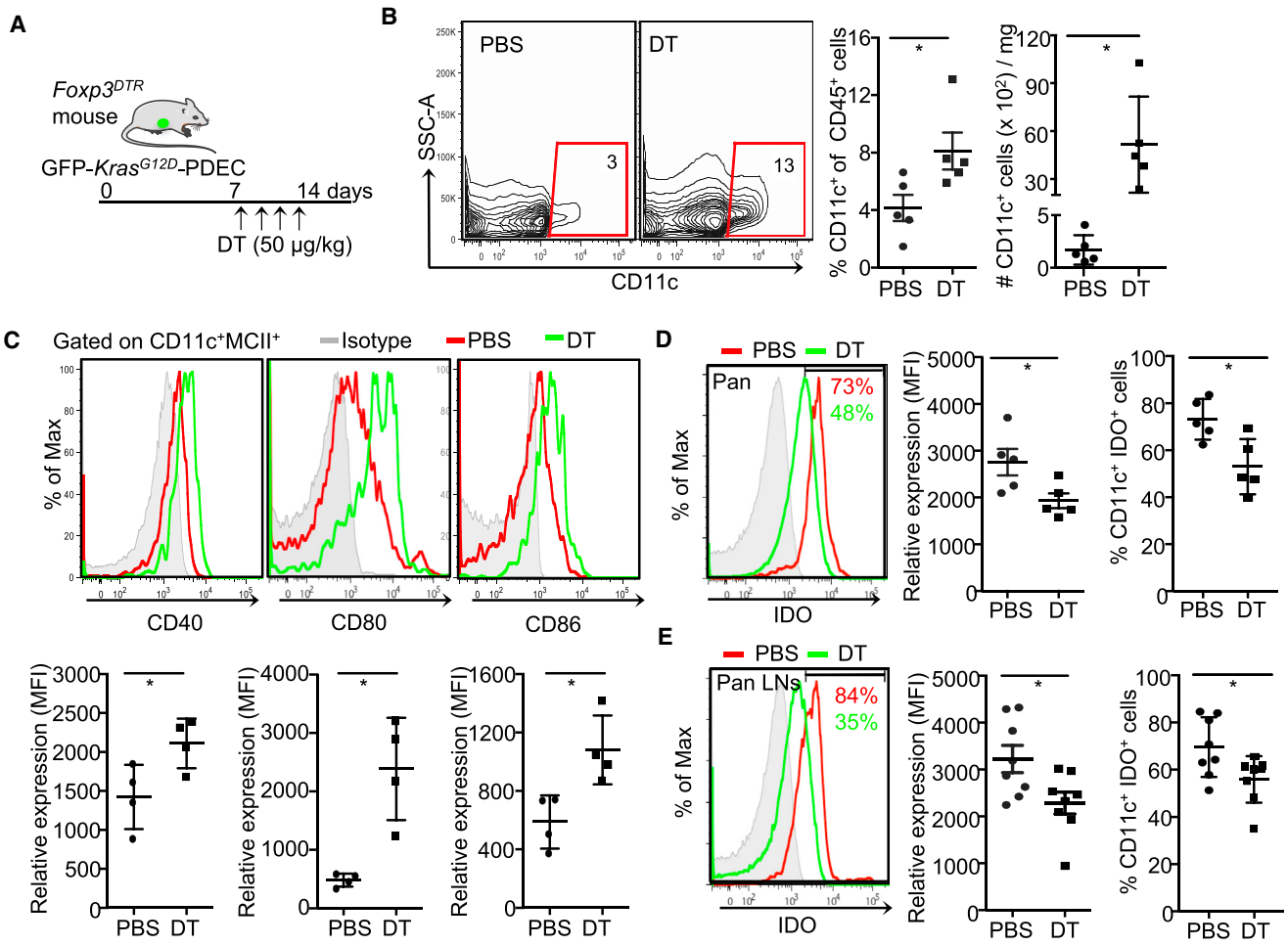

Figure 6. Treg Cell Ablation Changes the Frequency and Phenotype of Tumor-Associated CD11c$^+$ DCs in the Pancreatic TME

(A) Schematic of the experimental design. GFP-*Kras*^{G12D}-PDECs were implanted into the pancreata of syngeneic *Foxp3*^{DTR} mice, and either PBS or DT was injected as described in Figure 1E. Analyses were performed 14 days after orthotopic implantation.

(B) Flow cytometric plots (left) and quantification (right) of the percentage and number of CD11c$^+$ cells out of total CD45$^+$ cells (n = 5 mice).

(C) Relative surface expression levels of CD40, CD80, and CD86 on CD11c$^+$MHC class II$^+$ cells from orthotopic pancreatic grafts of *Foxp3*^{DTR} mice treated with either PBS (red) or DT (green) compared to respective isotype controls (gray) (n = 4 mice).

(D and E) Relative intracellular expression levels (left) and quantification of the percentage (right) of IDO in CD11c$^+$MHC class II$^+$ cells from pancreata (Pan) and Pan LNs of *Foxp3*^{DTR} mice treated with either PBS (red) or DT (green) compared to respective isotype controls (gray) (n = 5–8 mice).

Data are presented as mean ± SEM. *p < 0.05. See also Figure S6.

CTLA-4 expressed on Treg cells (Fallarino et al., 2003). The potential relevance of this mechanism to IDO expression in tumor-associated DCs is indicated by our observation that tumor-associated Treg cells display elevated levels of CTLA-4 compared to other lymphoid tissues. Intriguingly, IDO has been shown to modulate the immunosuppressive phenotype of Treg cells by controlling the levels of Akt signaling (Sharma et al., 2015), suggesting that the Treg cell-DC interaction in the TME may be involved in bidirectional communication. Thus, the establishment of immune tolerance in the pancreatic TME may in part be driven by a feed-forward mechanism involving the reciprocal interaction between DCs and Treg cells that mutually reinforces their immunosuppressive activities. Further insights from studies employing autochthonous mouse models of PDA as well as human PDA samples will be required to fully assess whether signal pathways that are downregulated in tumor-associated DCs through interactions with Treg cells can be therapeutically exploited to improve the anti-tumor immune response.

In summary, our study provides insights into Treg cell function in PDA progression. We demonstrate that Treg cells confer an immunosuppressive phenotype on tumor-associated CD11c$^+$ DCs that then fail to activate cytotoxic CD8$^+$ T cell-mediated delayed tumor growth. Targeting this series of interactions may provide a viable therapeutic strategy for the treatment of PDA.

EXPERIMENTAL PROCEDURES

Animals

The conditional *LSL-Kras*^{G12D} mice and *p48-Cre* mice were previously described (Pylayeva-Gupta et al., 2012). To perform lineage tracing, a

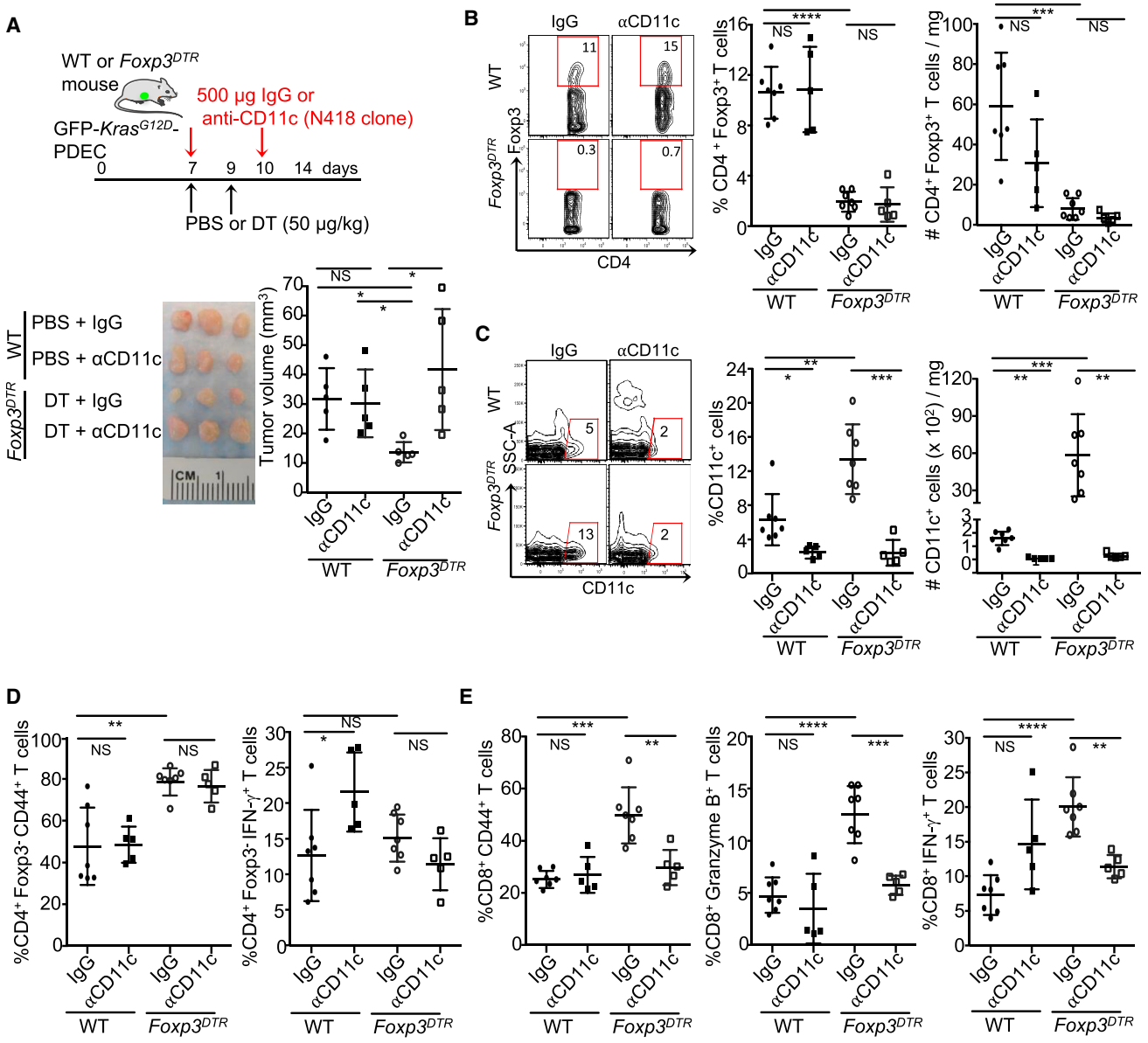

Figure 7. CD8⁺ T Cell Activation following Treg Cell Ablation Is Mediated by CD11c⁺ DCs

(A) Schematic of the experimental design. Orthotopic pancreatic grafts were analyzed by flow cytometry 14 days after implantation. Orthotopic pancreatic tumors (left) and quantification of tumor volume (right) (n = 5 mice).

(B and C) Flow cytometric plots and quantification (right) of the percentage and number of CD4⁺Foxp3⁺ Treg cells (B) and CD11c⁺ cells (C) (n = 4–5 mice).

(D and E) Quantification of expression of CD44 and IFN-γ in CD4⁺ Foxp3⁻ cells by flow cytometry (D) (n = 4–5 mice) and CD44, granzyme B, and IFN-γ in CD8⁺ T cells by flow cytometry (E) (n = 5–7 mice).

Data are presented as mean ± SEM. *p < 0.05, **p < 0.01, ***p < 0.001, ****p < 0.0001. NS, not significant. See also Figure S7.

Rosa^{tdTomato} reporter allele was introduced into *p48-Cre* and *p48-Cre*; *Kras*^{G12D} strains of mice to generate *p48-Cre*;*Rosa*^{tdTomato} (CT) and *p48-Cre*; *Kras*^{G12D};*Rosa*^{tdTomato} (KCT), respectively. *Foxp3-EGFP* (Bettelli et al., 2006), *CD11c-EYFP* (Lindquist et al., 2004), *Foxp3*^{DTR} (Kim et al., 2007), and *CD8a-Cre,* and *Rosa*^{tdTomto} mice were purchased from The Jackson Laboratory and C57BL/6 from National Cancer Institute (NCI) or Charles River Laboratories. *Foxp3-EGFP* or *CD8a-Cre;Rosa*^{tdtomato} female mice were crossed with *CD11c-EYFP* male mice to generate *Foxp3-EGFP;CD11c-EYFP* or *CD8a-Cre;Rosa*^{tdtomato}*;CD11c-EYFP* mice. All mice were on a C57BL/6 genetic background. The Institutional Animal Care and Use Committee at the New York University (NYU) School of Medicine approved all animal care and procedures.

Orthotopic Tumor Model

Isolation, culture, and adenoviral infection of PDECs was carried out as previously described (Pylayeva-Gupta et al., 2013). KPC cells isolated from KPC mice were a gift from Dr. R.H. Vonderheide (Byrne and Vonderheide, 2016; Lo et al., 2015). Orthotopic implantation is described in Supplemental Experiment Procedures. Tumor volume was calculated using the formula $\pi LW^2/6$.

In Vivo Treatments

For Treg cell ablation studies, DT (Sigma-Aldrich) was injected intraperitoneally (i.p.) at 50 μg per kg of body weight at the indicated times. For neutralization and depletion studies, anti-mouse IFN-γ (1 mg, clone XMG1.2, Bio X Cell), anti-mouse CD11c (500 μg, clone N418, Bio X Cell), anti-mouse CD8 (250 μg, clone 53-6.72, Bio X Cell), anti-mouse CD4 (150 μg, clone GK1.5, Bio X Cell), or anti-mouse CD25 (500 μg, clone PC-61.5.3, Bio X Cell) was injected i.p. at the indicated times. Isotype control antibodies used were rat IgG1, Armenian hamster IgG, or rat IgG2a from Bio X Cell, respectively.

Intravital TPLSM of Pancreas

Pancreata were prepared microsurgically for intravital microscopy. Mice were anaesthetized by an initial intraperitoneal injection of 100 mg/kg ketamine and 10 mg/kg xylazine and boosted with a half dose every 30–60 min. The spleen and pancreatic tail were externalized through a 1-cm left abdominal side incision, gently pulled out, and carefully fixed with a custom-made plastic apparatus, without inducing vascular damage. The mouse was then placed on the stage mounted with a coverslip so that the pancreas was in contact with the coverslip for imaging with an inverted objective. Detailed image acquisition and analysis are described in Supplemental Experimental Procedures.

Immunofluorescence

Mouse pancreata were harvested and fixed with 4% PFA for 1 hr at 4°C and cryoprotected with 30% sucrose for 18 hr. Fixed samples were then embedded in optimum cutting temperature (OCT) compound and snap frozen at −80°C until further processing.

The use of human tissue was reviewed and approved by the Institutional Review Board at the NYU School of Medicine and samples (provided by the Tissue Acquisition and Biorepository Service) were obtained with informed consent. 5-μm-thick sections from formalin-fixed paraffin-embedded samples were used for immunofluorescence staining. Detailed immunofluorescence, immunochemistry, H&E staining, and antibody information can be found in Supplemental Experimental Procedures.

Flow Cytometry

For mononuclear cell isolation, pancreata were minced into small fragments and incubated in collagenase V (1 mg/mL, Sigma) with DNase I (Roche) in RPMI-1640 at 37°C for 30 min with 150 rpm agitation. Dissociated cells were passed through a 70-μm cell strainer and washed with RPMI-1640 supplemented with 10% fetal calf serum (FCS). Total mononuclear cells were further purified by 47% Percoll (GE Healthcare) gradient centrifugation. Spleens and LNs were mechanically homogenized and passed through a 70-μm cell strainer. Red blood cells were lysed using ACK Lysis buffer (Lonza). Isolated cells were incubated with anti-CD16/CD32 antibody (BD PharMingen) to prevent non-specific antibody binding. Surface antigens were stained with the antibodies described in Supplemental Experimental Procedures. The corresponding isotype IgGs were stained. Dead cells were excluded using LIVE/DEAD Fixable Aqua Dead Cell Stain (Invitrogen). Multiparameter analysis was performed on a LSRII flow cytometer (BD Biosciences) and analyzed with FlowJo software (Tree Star). The geometric mean fluorescence intensity (MFI) was calculated as follows: MFI = MHC class II, CD40, CD80, or CD86 geometric mean − isotype geometric mean. Detailed Foxp3 and intracellular cytokine staining for flow cytometry and antibody information is described in Supplemental Experimental Procedures.

Statistical Analysis

All data are presented as mean ± SEM. Unpaired Student's t tests or nonparametric Mann-Whitney *U* tests were used to compare two variables as indicated in the figure legends. One-way analysis of variance (ANOVA) followed by Tukey's multiple comparison test was used for multiple-group comparison. Kaplan-Meier survival curves were calculated using the survival time of each mouse. The log-rank test was used to test for significant differences between two groups. Statistical analyses were performed with GraphPad Prism (GraphPad) (*$p < 0.05$, **$p < 0.01$, ***$p < 0.001$, ****$p < 0.0001$).

ACCESSION NUMBERS

The accession number for the flow cytometry data reported in this paper is FR: FR-FCM-ZY6U (http://flowrepository.org/id/RvFrgQpSRnJlgL61w5IphzuQvGkpc9zTHdf7xZVCSe6Q8apaQYQZcCW9VwpAJqLG).

SUPPLEMENTAL INFORMATION

Supplemental Information includes Supplemental Experimental Procedures, seven figures, and four movies and can be found with this article online at http://dx.doi.org/10.1016/j.celrep.2017.06.062.

AUTHOR CONTRIBUTIONS

J.-E.J., M.L.D., and D.B.-S. conceived and designed the experiments. J.-E.J. performed the experiments and analyzed the data. C.H.H. analyzed the mouse and human pancreatic samples, and C.L. provided RNA-sequencing data of $Kras^{G12D}$-PDECs. J.-E.J., G.M., M.L.D., and D.B.-S. wrote and reviewed the manuscript.

ACKNOWLEDGMENTS

We thank Y. Pylayeva-Gupta, L.J. Taylor, and J.S. Handler for discussions and help with manuscript preparation and the members of the Bar-Sagi laboratory for comments. We thank H. Beuneu for advice on two-photon microscopy of the pancreas. We also thank the NYUMC Office of Collaborative Science Cytometry Core and Histology Core, which are shared resources partially supported by Laura and Isaac Perlmutter Cancer Center support grant P30CA016087. The LSM710 microscope was purchased with support of NIH shared instrument grant S10 RR023704. This work was supported by NIH grant R01AI055037, the Wellcome Trust (PRF 100262Z/12/Z) (to M.L.D.), the NIH/NCI (CA210263), Project Purple, and Stand Up To Cancer – The Lustgarten Foundation Pancreatic Cancer Convergence Dream Team grant SU2C-AACR-DT14-14 (to D.B.S.). Stand Up To Cancer is a program of the Entertainment Industry Foundation administered by the American Association for Cancer Research.

Received: July 22, 2016
Revised: March 29, 2017
Accepted: June 21, 2017
Published: July 18, 2017

REFERENCES

Bauer, C.A., Kim, E.Y., Marangoni, F., Carrizosa, E., Claudio, N.M., and Mempel, T.R. (2014). Dynamic Treg interactions with intratumoral APCs promote local CTL dysfunction. J. Clin. Invest. *124*, 2425–2440.

Bayne, L.J., Beatty, G.L., Jhala, N., Clark, C.E., Rhim, A.D., Stanger, B.Z., and Vonderheide, R.H. (2012). Tumor-derived granulocyte-macrophage colony-stimulating factor regulates myeloid inflammation and T cell immunity in pancreatic cancer. Cancer Cell *21*, 822–835.

Bettelli, E., Carrier, Y., Gao, W., Korn, T., Strom, T.B., Oukka, M., Weiner, H.L., and Kuchroo, V.K. (2006). Reciprocal developmental pathways for the generation of pathogenic effector TH17 and regulatory T cells. Nature *441*, 235–238.

Boissonnas, A., Scholer-Dahirel, A., Simon-Blancal, V., Pace, L., Valet, F., Kissenpfennig, A., Sparwasser, T., Malissen, B., Fetler, L., and Amigorena, S. (2010). Foxp3+ T cells induce perforin-dependent dendritic cell death in tumor-draining lymph nodes. Immunity *32*, 266–278.

Bos, P.D., Plitas, G., Rudra, D., Lee, S.Y., and Rudensky, A.Y. (2013). Transient regulatory T cell ablation deters oncogene-driven breast cancer and enhances radiotherapy. J. Exp. Med. *210*, 2435–2466.

Byrne, K.T., and Vonderheide, R.H. (2016). CD40 stimulation obviates innate sensors and drives T cell immunity in cancer. Cell Rep. *15*, 2719–2732.

Cederbom, L., Hall, H., and Ivars, F. (2000). CD4+CD25+ regulatory T cells down-regulate co-stimulatory molecules on antigen-presenting cells. Eur. J. Immunol. *30*, 1538–1543.

Clark, C.E., Hingorani, S.R., Mick, R., Combs, C., Tuveson, D.A., and Vonderheide, R.H. (2007). Dynamics of the immune reaction to pancreatic cancer from inception to invasion. Cancer Res. *67*, 9518–9527.

Daley, D., Zambirinis, C.P., Seifert, L., Akkad, N., Mohan, N., Werba, G., Barilla, R., Torres-Hernandez, A., Hundeyin, M., Mani, V.R., et al. (2016). γδ T cells support pancreatic oncogenesis by restraining αβ T cell activation. Cell *166*, 1485–1499.

Darrasse-Jèze, G., Bergot, A.S., Durgeau, A., Billiard, F., Salomon, B.L., Cohen, J.L., Bellier, B., Podsypanina, K., and Klatzmann, D. (2009). Tumor emergence is sensed by self-specific CD44hi memory Tregs that create a dominant tolerogenic environment for tumors in mice. J. Clin. Invest. *119*, 2648–2662.

Delgoffe, G.M., Woo, S.R., Turnis, M.E., Gravano, D.M., Guy, C., Overacre, A.E., Bettini, M.L., Vogel, P., Finkelstein, D., Bonnevier, J., et al. (2013). Stability and function of regulatory T cells is maintained by a neuropilin-1-semaphorin-4a axis. Nature *501*, 252–256.

Fallarino, F., Grohmann, U., Hwang, K.W., Orabona, C., Vacca, C., Bianchi, R., Belladonna, M.L., Fioretti, M.C., Alegre, M.L., and Puccetti, P. (2003). Modulation of tryptophan catabolism by regulatory T cells. Nat. Immunol. *4*, 1206–1212.

Ghiringhelli, F., Puig, P.E., Roux, S., Parcellier, A., Schmitt, E., Solary, E., Kroemer, G., Martin, F., Chauffert, B., and Zitvogel, L. (2005). Tumor cells convert immature myeloid dendritic cells into TGF-beta-secreting cells inducing CD4+CD25+ regulatory T cell proliferation. J. Exp. Med. *202*, 919–929.

Guerra, C., Schuhmacher, A.J., Cañamero, M., Grippo, P.J., Verdaguer, L., Pérez-Gallego, L., Dubus, P., Sandgren, E.P., and Barbacid, M. (2007). Chronic pancreatitis is essential for induction of pancreatic ductal adenocarcinoma by K-Ras oncogenes in adult mice. Cancer Cell *11*, 291–302.

Hansen, W., Hutzler, M., Abel, S., Alter, C., Stockmann, C., Kliche, S., Albert, J., Sparwasser, T., Sakaguchi, S., Westendorf, A.M., et al. (2012). Neuropilin 1 deficiency on CD4+Foxp3+ regulatory T cells impairs mouse melanoma growth. J. Exp. Med. *209*, 2001–2016.

Hiraoka, N., Onozato, K., Kosuge, T., and Hirohashi, S. (2006). Prevalence of FOXP3+ regulatory T cells increases during the progression of pancreatic ductal adenocarcinoma and its premalignant lesions. Clin. Cancer Res. *12*, 5423–5434.

Hori, S., Nomura, T., and Sakaguchi, S. (2003). Control of regulatory T cell development by the transcription factor Foxp3. Science *299*, 1057–1061.

Josefowicz, S.Z., Lu, L.F., and Rudensky, A.Y. (2012). Regulatory T cells: mechanisms of differentiation and function. Annu. Rev. Immunol. *30*, 531–564.

Joshi, N.S., Akama-Garren, E.H., Lu, Y., Lee, D.Y., Chang, G.P., Li, A., DuPage, M., Tammela, T., Kerper, N.R., Farago, A.F., et al. (2015). Regulatory T Cells in Tumor-Associated Tertiary Lymphoid Structures Suppress Anti-tumor T Cell Responses. Immunity *43*, 579–590.

Keenan, B.P., Saenger, Y., Kafrouni, M.I., Leubner, A., Lauer, P., Maitra, A., Rucki, A.A., Gunderson, A.J., Coussens, L.M., Brockstedt, D.G., et al. (2014). A Listeria vaccine and depletion of T-regulatory cells activate immunity against early stage pancreatic intraepithelial neoplasms and prolong survival of mice. Gastroenterology *146*, 1784–1794.

Keir, M.E., Butte, M.J., Freeman, G.J., and Sharpe, A.H. (2008). PD-1 and its ligands in tolerance and immunity. Annu. Rev. Immunol. *26*, 677–704.

Kim, J.M., Rasmussen, J.P., and Rudensky, A.Y. (2007). Regulatory T cells prevent catastrophic autoimmunity throughout the lifespan of mice. Nat. Immunol. *8*, 191–197.

Larmonier, N., Marron, M., Zeng, Y., Cantrell, J., Romanoski, A., Sepassi, M., Thompson, S., Chen, X., Andreansky, S., and Katsanis, E. (2007). Tumor-derived CD4(+)CD25(+) regulatory T cell suppression of dendritic cell function involves TGF-beta and IL-10. Cancer Immunol. Immunother. *56*, 48–59.

Leao, I.C., Ganesan, P., Armstrong, T.D., and Jaffee, E.M. (2008). Effective depletion of regulatory T cells allows the recruitment of mesothelin-specific CD8 T cells to the antitumor immune response against a mesothelin-expressing mouse pancreatic adenocarcinoma. Clin. Transl. Sci. *1*, 228–239.

Lindquist, R.L., Shakhar, G., Dudziak, D., Wardemann, H., Eisenreich, T., Dustin, M.L., and Nussenzweig, M.C. (2004). Visualizing dendritic cell networks in vivo. Nat. Immunol. *5*, 1243–1250.

Lo, A., Wang, L.C., Scholler, J., Monslow, J., Avery, D., Newick, K., O'Brien, S., Evans, R.A., Bajor, D.J., Clendenin, C., et al. (2015). Tumor-promoting desmoplasia is disrupted by depleting FAP-expressing stromal cells. Cancer Res. *75*, 2800–2810.

Lunardi, S., Lim, S.Y., Muschel, R.J., and Brunner, T.B. (2015). IP-10/CXCL10 attracts regulatory T cells: Implication for pancreatic cancer. OncoImmunology *4*, e1027473.

Maldonado, R.A., and von Andrian, U.H. (2010). How tolerogenic dendritic cells induce regulatory T cells. Adv. Immunol. *108*, 111–165.

Markowitz, J., Brooks, T.R., Duggan, M.C., Paul, B.K., Pan, X., Wei, L., Abrams, Z., Luedke, E., Lesinski, G.B., Mundy-Bosse, B., et al. (2015). Patients with pancreatic adenocarcinoma exhibit elevated levels of myeloid-derived suppressor cells upon progression of disease. Cancer Immunol. Immunother. *64*, 149–159.

Munn, D.H., and Mellor, A.L. (2016). IDO in the tumor microenvironment: inflammation, counter-regulation, and tolerance. Trends Immunol. *37*, 193–207.

Munn, D.H., Sharma, M.D., Lee, J.R., Jhaver, K.G., Johnson, T.S., Keskin, D.B., Marshall, B., Chandler, P., Antonia, S.J., Burgess, R., et al. (2002). Potential regulatory function of human dendritic cells expressing indoleamine 2,3-dioxygenase. Science *297*, 1867–1870.

Nishikawa, H., and Sakaguchi, S. (2010). Regulatory T cells in tumor immunity. Int. J. Cancer *127*, 759–767.

Onishi, Y., Fehervari, Z., Yamaguchi, T., and Sakaguchi, S. (2008). Foxp3+ natural regulatory T cells preferentially form aggregates on dendritic cells in vitro and actively inhibit their maturation. Proc. Natl. Acad. Sci. USA *105*, 10113–10118.

Pinzon-Charry, A., Maxwell, T., and López, J.A. (2005). Dendritic cell dysfunction in cancer: a mechanism for immunosuppression. Immunol. Cell Biol. *83*, 451–461.

Pylayeva-Gupta, Y., Lee, K.E., Hajdu, C.H., Miller, G., and Bar-Sagi, D. (2012). Oncogenic Kras-induced GM-CSF production promotes the development of pancreatic neoplasia. Cancer Cell *21*, 836–847.

Pylayeva-Gupta, Y., Lee, K.E., and Bar-Sagi, D. (2013). Microdissection and culture of murine pancreatic ductal epithelial cells. Methods Mol. Biol. *980*, 267–279.

Qureshi, O.S., Zheng, Y., Nakamura, K., Attridge, K., Manzotti, C., Schmidt, E.M., Baker, J., Jeffery, L.E., Kaur, S., Briggs, Z., et al. (2011). Trans-endocytosis of CD80 and CD86: a molecular basis for the cell-extrinsic function of CTLA-4. Science *332*, 600–603.

Ryan, D.P., Hong, T.S., and Bardeesy, N. (2014). Pancreatic adenocarcinoma. N. Engl. J. Med. *371*, 1039–1049.

Sarris, M., Andersen, K.G., Randow, F., Mayr, L., and Betz, A.G. (2008). Neuropilin-1 expression on regulatory T cells enhances their interactions with dendritic cells during antigen recognition. Immunity *28*, 402–413.

Scarlett, U.K., Rutkowski, M.R., Rauwerdink, A.M., Fields, J., Escovar-Fadul, X., Baird, J., Cubillos-Ruiz, J.R., Jacobs, A.C., Gonzalez, J.L., Weaver, J., et al. (2012). Ovarian cancer progression is controlled by phenotypic changes in dendritic cells. J. Exp. Med. *209*, 495–506.

Schildknecht, A., Brauer, S., Brenner, C., Lahl, K., Schild, H., Sparwasser, T., Probst, H.C., and van den Broek, M. (2010). FoxP3+ regulatory T cells essentially contribute to peripheral CD8+ T-cell tolerance induced by steady-state dendritic cells. Proc. Natl. Acad. Sci. USA *107*, 199–203.

Schlecker, E., Stojanovic, A., Eisen, C., Quack, C., Falk, C.S., Umansky, V., and Cerwenka, A. (2012). Tumor-infiltrating monocytic myeloid-derived suppressor cells mediate CCR5-dependent recruitment of regulatory T cells favoring tumor growth. J. Immunol. *189*, 5602–5611.

Shang, B., Liu, Y., Jiang, S.J., and Liu, Y. (2015). Prognostic value of tumor-infiltrating FoxP3+ regulatory T cells in cancers: a systematic review and meta-analysis. Sci. Rep. *5*, 15179.

Shankaran, V., Ikeda, H., Bruce, A.T., White, J.M., Swanson, P.E., Old, L.J., and Schreiber, R.D. (2001). IFNgamma and lymphocytes prevent primary tumour development and shape tumour immunogenicity. Nature *410*, 1107–1111.

Sharma, M.D., Baban, B., Chandler, P., Hou, D.Y., Singh, N., Yagita, H., Azuma, M., Blazar, B.R., Mellor, A.L., and Munn, D.H. (2007). Plasmacytoid dendritic cells from mouse tumor-draining lymph nodes directly activate mature Tregs via indoleamine 2,3-dioxygenase. J. Clin. Invest. *117*, 2570–2582.

Sharma, M.D., Shinde, R., McGaha, T.L., Huang, L., Holmgaard, R.B., Wolchok, J.D., Mautino, M.R., Celis, E., Sharpe, A.H., Francisco, L.M., and et al. (2015). The PTEN pathway in Tregs is a critical driver of the suppressive tumor microenvironment. Sci. Adv. *1*, e1500845.

Steinman, R.M., Hawiger, D., and Nussenzweig, M.C. (2003). Tolerogenic dendritic cells. Annu. Rev. Immunol. *21*, 685–711.

Stromnes, I.M., DelGiorno, K.E., Greenberg, P.D., and Hingorani, S.R. (2014). Stromal reengineering to treat pancreas cancer. Carcinogenesis *35*, 1451–1460.

Tan, M.C., Goedegebuure, P.S., Belt, B.A., Flaherty, B., Sankpal, N., Gillanders, W.E., Eberlein, T.J., Hsieh, C.S., and Linehan, D.C. (2009). Disruption of CCR5-dependent homing of regulatory T cells inhibits tumor growth in a murine model of pancreatic cancer. J. Immunol. *182*, 1746–1755.

Tang, Q., Adams, J.Y., Tooley, A.J., Bi, M., Fife, B.T., Serra, P., Santamaria, P., Locksley, R.M., Krummel, M.F., and Bluestone, J.A. (2006). Visualizing regulatory T cell control of autoimmune responses in nonobese diabetic mice. Nat. Immunol. *7*, 83–92.

Tang, Y., Xu, X., Guo, S., Zhang, C., Tang, Y., Tian, Y., Ni, B., Lu, B., and Wang, H. (2014). An increased abundance of tumor-infiltrating regulatory T cells is correlated with the progression and prognosis of pancreatic ductal adenocarcinoma. PLoS ONE *9*, e91551.

Teng, M.W., Ngiow, S.F., von Scheidt, B., McLaughlin, N., Sparwasser, T., and Smyth, M.J. (2010). Conditional regulatory T-cell depletion releases adaptive immunity preventing carcinogenesis and suppressing established tumor growth. Cancer Res. *70*, 7800–7809.

Vonderheide, R.H., and Bayne, L.J. (2013). Inflammatory networks and immune surveillance of pancreatic carcinoma. Curr. Opin. Immunol. *25*, 200–205.

Weiss, J.M., Bilate, A.M., Gobert, M., Ding, Y., Curotto de Lafaille, M.A., Parkhurst, C.N., Xiong, H., Dolpady, J., Frey, A.B., Ruocco, M.G., et al. (2012). Neuropilin 1 is expressed on thymus-derived natural regulatory T cells, but not mucosa-generated induced Foxp3+ T reg cells. J. Exp. Med. *209*, 1723–1742.

Wing, K., Onishi, Y., Prieto-Martin, P., Yamaguchi, T., Miyara, M., Fehervari, Z., Nomura, T., and Sakaguchi, S. (2008). CTLA-4 control over Foxp3+ regulatory T cell function. Science *322*, 271–275.

Yang, A.S., and Lattime, E.C. (2003). Tumor-induced interleukin 10 suppresses the ability of splenic dendritic cells to stimulate CD4 and CD8 T-cell responses. Cancer Res. *63*, 2150–2157.